Paper
Int'l J. of Aeronautical & Space Sci. 16(4), 614–623 (2015)
DOI: http://dx.doi.org/10.5139/IJASS.2015.16.4.614

IJASS
International Journal of Aeronautical and Space Sciences

Inflow Prediction and First Principles Modeling of a Coaxial Rotor Unmanned Aerial Vehicle in Forward Flight

Mohammad Harun-Or-Rashid*, Jun-Beom Song, Young-Seop Byun*** and Beom-Soo Kang******

Department of Aerospace Engineering, Pusan National University, Busan 46241, Republic of Korea

Abstract

When the speed of a coaxial rotor helicopter in forward flight increases, the wake skew angle of the rotor increases and consequently the position of the vena contracta of the upper rotor with respect to the lower rotor changes. Considering ambient air and the effect of the upper rotor, this study proposes a nonuniform inflow model for the lower rotor of a coaxial rotor helicopter in forward flight. The total required power of the coaxial rotor system was compared against Dingeldein's experimental data, and the results of the proposed model were well matched. A plant model was also developed from first principles for flight simulation, unknown parameter estimation and control analysis. The coaxial rotor helicopter used for this study was manufactured for surveillance and reconnaissance and does not have any stabilizer bar. Therefore, a feedback controller was included during flight test and parameter estimation to overcome unstable situations. Predicted responses of parameter estimation and validation show good agreement with experimental data. Therefore, the methodology described in this paper can be used to develop numerical plant model, study non-uniform inflow model, conduct performance analysis and parameter estimation of coaxial rotor as well as other rotorcrafts in forward flight.

Key words: blade element theory, coaxial rotor, forward flight, nonuniform inflow

1. Introduction

A coaxial rotor system has two concentric counter-rotating rotors to produce lift and balance the torque. A tail rotor is therefore not necessary. The coaxial rotor helicopter is easy to stabilize and control because of its aerodynamic symmetry.

The nondimensional quantity of air inflow can be considered as uniformly distributed over the rotor disk to avoid complexity. However, because of the geometry of the blade (twist), blade flapping, change of tip speed along the blade radius, generation of vortices and unsteady flow, and rotation of the blade through 0°–360° azimuth, the inflow distribution is in reality nonuniform. Therefore, in this study, nonuniform inflow is considered. In 1926, Glauert [1] proposed a first harmonic nonuniform inflow model. Longitudinal and lateral weighting factors considered in Glauert's inflow model that were analytically determined by many scholars, including Coleman et al. (1945), Drees (1949), White and Blake (1979), and Pitt and Peters (1981), on the basis of experimental data, are very useful in the field of aerodynamics for rotor performance analysis [1, 2]. In the present study, Coleman's longitudinal and lateral weighting factors are used for both upper and lower rotor inflow analyses and an inflow model is suggested for the lower rotor.

Parameter estimation is a curve-fitting technique where a cost function is used to minimize the fitting errors of the experimental data and predicted responses of the plant. Many studies have been carried out where stability and control derivatives of the state space model are estimated for both helicopter and fixed wing aircraft.

* Ph. D Student
** Researcher
*** Ph. D Student
**** Professor, Corresponding author: bskang@pusan.ac.kr

Received: April 20, 2015 Revised: December, 11, 2015 Accepted: December 20, 2015

http://ijass.org pISSN: 2093-274x eISSN: 2093-2480

Such as Mettler et al. and Valavanis identified quasi-steady derivatives and physical parameters of the single rotor unmanned aerial vehicle (UAV) by using the Comprehensive Identification from FrEquency Responses (CIFER) tool, and developed their controller on the basis of the identified state space model; Kenneth explained the parameter estimation of an aircraft [3-9]. Conversely, very few studies have been conducted on parameter estimation and system identification of small coaxial rotor helicopters. Furthermore, there is a lack of work on lower rotor inflow in the forward flight case. Therefore, the main motivation of this study was to propose an inflow model for the lower rotor of the coaxial rotor helicopter, determine the required power and identify unknown parameters, which cannot be measured directly on the basis of experimental results and the predicted responses from a non-linear mathematical model of the plant in forward flight.

We describe the development of a mathematical model of a coaxial rotor helicopter, using a first principles approach that is based on basic helicopter theory. In this approach, thrust and torque were calculated by advanced blade element theory (BET) rather than simple momentum theory. An inflow model is also proposed for the lower rotor of the coaxial rotor helicopter. The proposed model was validated against the widely used experimental data of Dingeldein by incorporating the model into the numerical code. In this study, experiments were conducted in forward flight. Unknown parameters were estimated and validated on the basis of time domain experimental data.

Nomenclature

C_l	lift coefficient
N_s	number of segments
p, q, r	angular velocities around x, y, z axes (rad.s^{-1})
X_{SA}	skew angle (rad.)
σ	rotor solidity
λ_a	tip speed ratio
ψ_a	azimuth angle (rad.)
θ_{col}	collective angle (rad.)

Subscripts:

i	induced
l	lower rotor
u	upper rotor

2. Description of the Code

Coaxial rotor dynamics is very complex because the high-speed downstream and wake of the upper rotor influence the lower rotor. A number of methods, such as blade element momentum theory (BEMT), momentum theory, and BET, are generally used for rotor performance analysis. In the hover condition, dynamic behavior predicted by BEMT shows better results than simple momentum theory when compared with experimental data [10]. However, even though BEMT shows better results, BET is used for this study because with BEMT it is assumed that the inflow is the same at different azimuth angles for a selected radial distance. On the other hand, in the case of BET, inflow changes with azimuth angle. Moreover, the literature on BEMT specifically covers hover and axial flight, whereas this study focuses on forward flight.

We used the following procedure. First, different linear nonuniform inflow models were analyzed. Subsequently, the best-fitted longitudinal and lateral weighting factors were used to predict the thrust and torque produced by the upper rotor. An inflow model for the lower rotor was then developed and the thrust and torque were predicted. Finally, unknown parameters for the coaxial rotor helicopter were identified by using flight test data.

Figure 1 shows the configuration of a coaxial rotor helicopter; Fig. 2 presents a flowchart of the process followed to calculate thrust and torque coefficients C_T and C_p, respectively. During numerical simulation, the rotor blade was divided into 100 segments. In this study, the thrust coefficient for the rotor, C_T, is calculated by means of BET. The inflow ratio (λ) can be estimated in different ways, including by determining blade forces or by using different inflow models available in helicopter aerodynamics [1]. In the first case, the out-of-plane and in-plane components of velocity are determined. Inflow is the ratio of the out-of-plane and in-plane components of velocity as well as a function of the radial position of the blade under consideration. In the

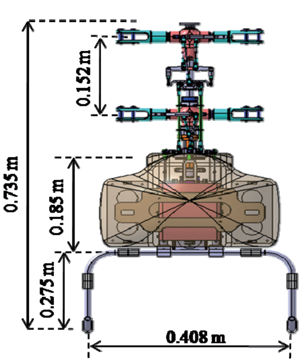

Fig. 1. Coaxial rotor helicopter

second case, Glauert's basic inflow model in forward flight is used where longitudinal and lateral weighting factors represent the distinction of the present nonuniform inflow model (λ_u) from the uniform inflow model (λ_0) derived by momentum theory. This model was applied for calculating the inflow of the upper rotor in forward flight. Glauert's inflow equation is

$$\lambda_u = \lambda_0(1 + K_x^{lon} r\cos\psi_a + K_y^{lat} r\sin\psi_a) + (\lambda_\alpha / 2)^2 \quad (1)$$

where K_x^{lon} and K_y^{lat} are the longitudinal and lateral weighting factors, respectively, and r (= $y/R \le 1$) is the nondimensional radial position of the blade element. Weighting factors proposed by Coleman are

$$K_x^{lon} = \tan(X_{SA} / 2) \quad (2)$$

$$K_y^{lat} = 0 \quad (3)$$

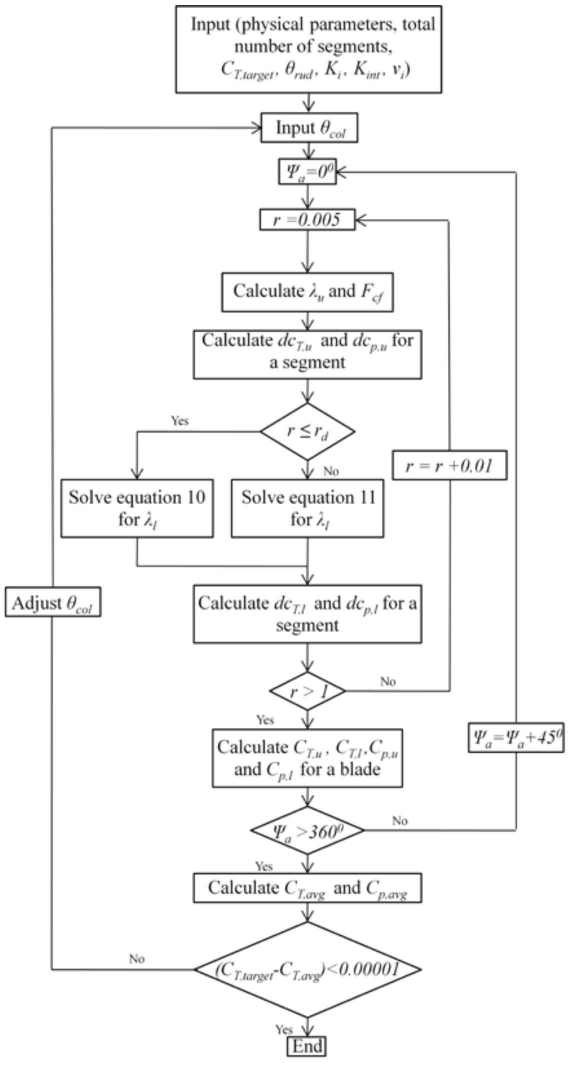

Fig. 2. Flow chart to estimate thrust and torque coefficients

Figure 3 shows the induced power comparison deduced by using different inflow models against the theoretical data of Prouty [11]. It was found that the results of Coleman's model gave the best fit to the theoretical data. At high speed, all inflow models show discrepancies, among which the constant momentum induced velocity case shows maximum discrepancy because it is more suited to the low-speed condition.

Figure 4 shows a comparison of different inflow models with the inflow measurements of Elliott et al. (1988), for both longitudinal and lateral coordinates [12]. According to Elliott et al., rectangular and linear twisted blades were used and measurements were made by laser velocimeter (LV) one chord height above the tip path plane (TPP). Because a forward flight experiment was conducted, the rotor shaft was tilted for the trim condition. During the test, a rotor rotational speed of 2113 rpm was maintained and the nominal thrust coefficient was 0.0064. Fig. 4(a) shows that the major inconsistencies are near the rotor hub and at the tip because of the fuselage below the rotor hub and generation of vortices near the tip. In forward flight, inflow at the leading edge of the disk is less than at the tailing edge; experimental data show that at low speed flight inflow is negative near the tip at azimuth angle ψ_a = 180°, but increases and becomes positive at high speed. Fig. 4(b) shows the inflow distribution at advance ratio μ = 0.23. Fig. 4(c) and (d) show nonuniform as well as uniform inflow distribution. The results of Coleman's model show uniform inflow because the lateral weighting factor K_y^{lat} = 0. If it is assumed that $K_y^{lat} = -2\mu$, as in the Drees model, then inflow results become linear nonuniform. However, from experimental data, it is clear that for lateral coordinates the inflow distribution is approximately symmetric. In the case of a single rotor helicopter, a swash plate mechanism provides more collective angle at an azimuth angle of 270° than at an azimuth angle of 90° and produces the same thrust, whereas a coaxial rotor helicopter uses two counter-

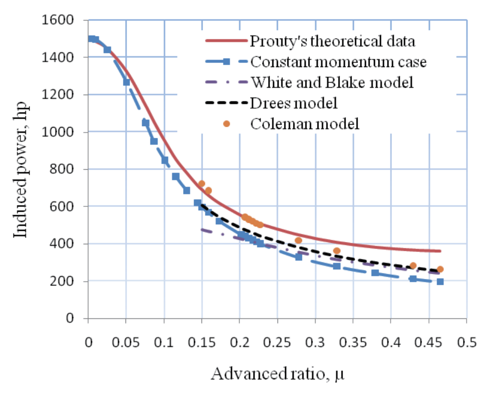

Fig. 3. Predicted induced power of upper rotor

DOI: http://dx.doi.org/10.5139/IJASS.2015.16.4.614

rotating rotors and swash plate mechanisms to minimize the lift difference between the advancing and retreating sides and to maintain symmetric lift distribution and lateral stability. Therefore, in this study, Coleman's model was used where the lateral weighting factor is zero; this model is also easier to implement in code than other models such as the Mangler and Squire method and the vortex method.

After the inflow ratio calculation was completed, the segment thrust and power coefficients, dc_T and dc_p, were estimated. The required induced power is proportional to the blade angle of attack and inversely proportional to the airspeed; that is, induced power is directly influenced by inflow, whereas profile power is proportional to the frictional resistance of the blade and airspeed. The BET code presented here is capable of taking into consideration blade twist and taper. The blade's section thrust, and the induced and profile power coefficients are calculated with Eqs. (4)–(6), respectively [1].

$$dc_{T,u} = \frac{\sigma a_0}{2} F_{cf}[\theta_{col,u} - \frac{\lambda_u}{r}]r^2 dr \tag{4}$$

$$dc_{p_i,u} = KK_{\text{int}}\frac{\sigma}{2}(\lambda_u C_l r^2)dr \tag{5}$$

$$dc_{p_p,u} = \frac{\sigma}{2}[\int_0^1 C_{d0} r^3 dr + \int_0^1 D_1(\theta_{col,u} - \phi_u) r^3 dr + \int_0^1 D_2(\theta_{col,u} - \phi_u)^2 r^3 dr] \tag{6}$$

Here, F_{cf} is the Prandtl tip loss factor, K is the induced power factor that incorporates actual effects such as tip losses and swirl effect, K_{int} is the induced power interference factor, ϕ_u (λ_u/r) is the induced inflow angle, and D_1 and D_2 are the drag coefficients. At the tip of each blade, vortices are formed that produce local inflow. As a result, lifting potential is reduced near the tips. This tip loss is considered by incorporating the Prandtl tip loss factor in the thrust coefficient equation. The Prandtl tip loss factor can be described as follows [1]:

$$F_{cf} = \left(2/\pi\right)\cos^{-1}\left(\exp\left(-\frac{N_b}{2}.\frac{1-r}{\lambda_u}\right)\right) \tag{7}$$

where the number of blades in each rotor N_b = 2. Thrust and power coefficients were calculated for all segments separately. Subsequently, total thrust and power coefficients of the upper rotor were estimated with Eqs. (8) and (9), respectively [10].

$$C_{T,u} = \sum_{n=1}^{N_s} dc_{T,u,n} \tag{8}$$

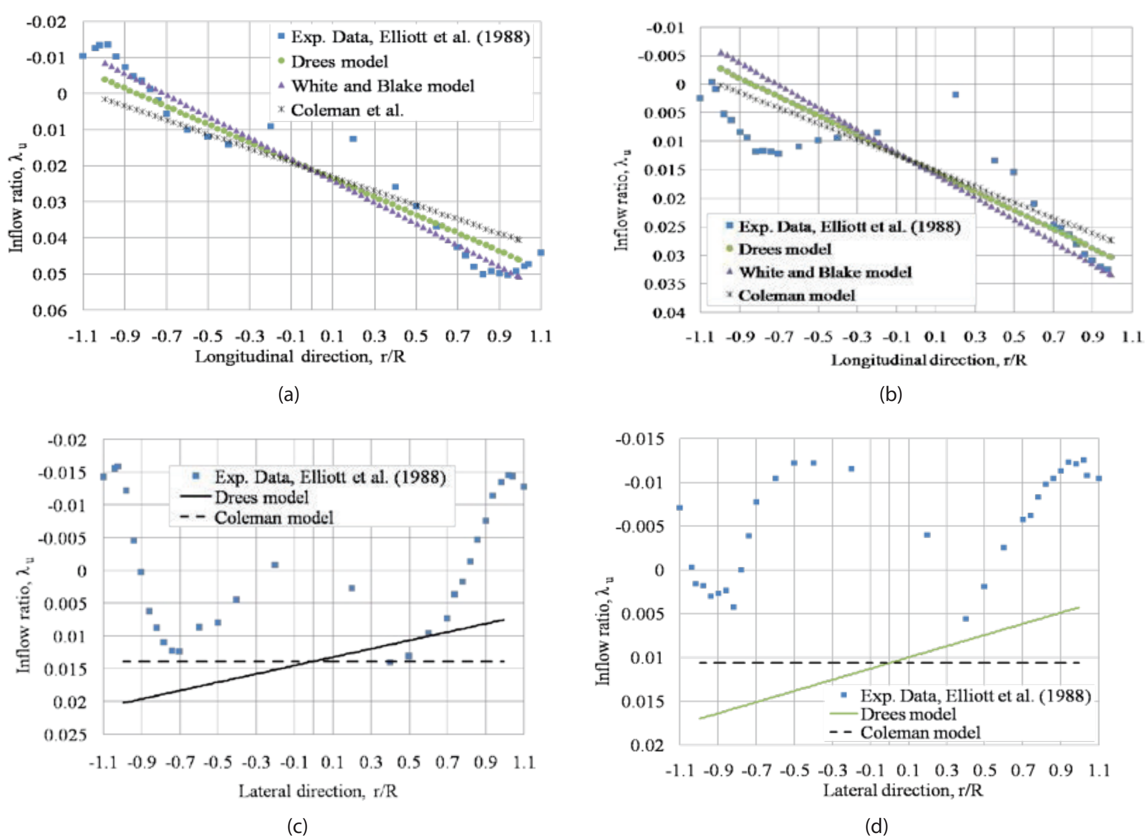

Fig. 4. Experimental and theoretical data comparison of mean longitudinal inflow ratio at (a) μ= 0.15, (b) μ= 0.23; Experimental and theoretical data comparison of mean lateral inflow ratio, at (c) μ= 0.23, (d) μ= 0.3.

$$C_{p,u} = \sum_{n=1}^{N_s} (dc_{p_i,u,n} + dc_{p_p,u,n}) \tag{9}$$

Finally, the upper rotor thrust, $T_u = C_{T,u}\rho A_u(\Omega R_u)^2$, and the torque, $Q_u = C_{Q,u}\rho A_u(\Omega R_u)^2 R_u$ (with torque coefficient, $C_{Q,u} \equiv C_{p,u}$) were calculated.

The lower rotor was placed at the vena contracta of the upper rotor. The nondimensional radial distance r_d of the vena contracta is equal to 0.7071 when it is fully contracted. However, in the hover condition, if it is assumed that the wake of the upper rotor influences the lower rotor up to 82% from its center point, then it shows better agreement [10]. In this study, it was found that r_d = 0.82 is not reasonable when the helicopter is in the forward flight condition. In forward flight, the rotor wake skew angle increases as the speed increases. As a result, the vena contracta moves backward. The shape of the vena contracta also changes. Since the position of the vena contracta changes with helicopter speed, r_d is a function of speed. Therefore, it was assumed that $r_d = 0.8–1.849\mu$ (advance ratio from 0.007 to 0.3) when the azimuth angle is 180° and reaches 1 at an azimuth angle of 0°. The backwash of the upper rotor flows through A_d, the area of the lower rotor. As a result, the inflow ratio of this area will be different from the unaffected disk area. In this study, the upper rotor's downstream and free stream velocity effects are considered. If $r \le r_d$, then the inflow distribution in forward flight is

$$\lambda_l = \lambda_0(1 + K_x^{lon} r\cos\psi_a + K_y^{lat} r\sin\psi_a) + (\lambda_u/2) + (\lambda_\alpha/2)^2 \tag{10}$$

Eq. (10) is proposed for the prediction of the lower rotor inflow. This equation is applicable for the region that is affected by the downstream of the upper rotor. Here, the second term ($\lambda_u/2$) on the right-hand side shows the influence of the upper rotor on the lower rotor. In contrast, if $r > r_d$, then the inflow distribution is

$$\lambda_l = \lambda_0(1 + K_x^{lon} r\cos\psi_a + K_y^{lat} r\sin\psi_a) + (\lambda_\alpha/2)^2 \tag{11}$$

which is the same as the inflow calculation of the upper rotor. For this condition, only clean air influences the disk. Fig. 5(a) shows the position of the vena contracta in hover mode and Fig. 5(b) illustrates the position in forward flight. Because this study focuses on the forward flight condition,

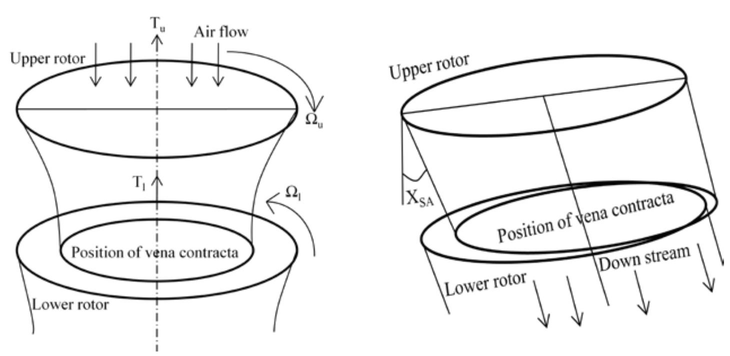

(a) (b)

Fig. 5. (a) Hover mode, (b) position of the vena contracta in forward flight

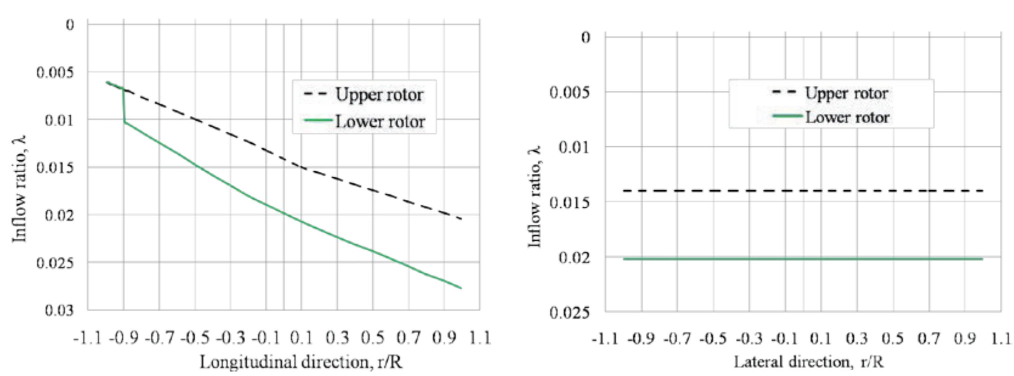

(a) (b)

Fig. 6. Coaxial rotor helicopter inflow distribution in (a) longitudinal and (b) lateral direction at μ= 0.15

the hover mode will not be discussed in detail.

Figure 6 shows the predicted inflow distributions of the upper and lower rotors in the longitudinal and lateral directions (Harrington rotor 1: C_T = 0.0048, solidity, σ = 0.054). Except for the small portion at an azimuth angle ψ_a = 180° (Fig. 6(a)), the inflow for both cases at the lower rotor is higher than for the upper rotor because the lower rotor is affected by the downstream of the upper rotor. As a result, the thrust and torque produced by the upper rotor become greater than those produced by the lower rotor. Therefore, the lower rotor must maintain a higher collective angle to balance the torque (Fig. 7(a)). In the case of the coaxial rotor helicopter, the upper and lower rotors are connected to each other by a linkage (Fig. 7(b)). The manufactured helicopter model is fitted with an actuator for changing the collective angle of both rotors simultaneously and an actuator for altering the collective angle of the lower rotor only to produce the same torque as the upper rotor, but in the opposite direction. The rudder input is the difference in the blade pitch angles between the lower and upper rotors ($\theta_{rud} = \theta_{col,l} - \theta_{col,u}$); the heading of the helicopter is changed by varying this value.

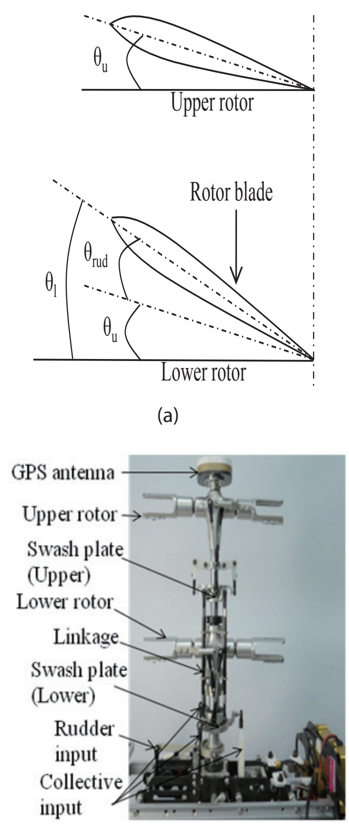

(a)

(b)

Fig. 7. Collective control and swash plate mechanism

Figure 8 shows a comparison between the predicted results of momentum theory, BET, the proposed inflow model, and experimental data of a coaxial rotor helicopter at a thrust coefficient of 0.0048 in forward flight [1, 13, 14]. Both the induced power and profile power were estimated by simple momentum theory as well as by BET. The thrust and power coefficients of the lower rotor were calculated by the proposed inflow model. The results of BET, with the developed inflow model included, show better agreement with the experimental data than those obtained with momentum theory. The required power of the coaxial rotor is higher than that of an equivalent single rotor because of the interference effects and drag losses of the two rotors. The installed motor power of the developed unmanned coaxial rotor helicopter is 3.0 hp, whereas the estimated power consumption is 2.8 hp at μ = 0.1 and K_{int} = 1.35. This indicates a good prediction capability of the numerical code.

Figure 9 shows the roll controller of the developed plant model where roll command, roll angle, and roll rate are

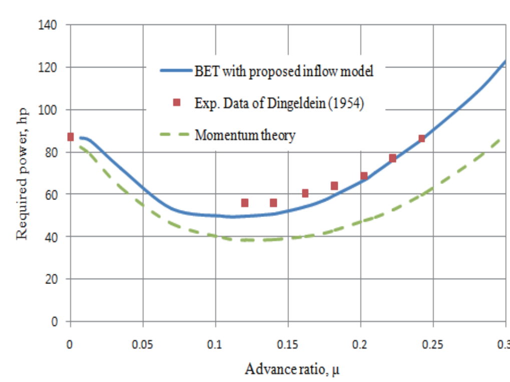

Fig. 8. Coaxial rotor helicopter power prediction in forward flight, Dingeldein 1954

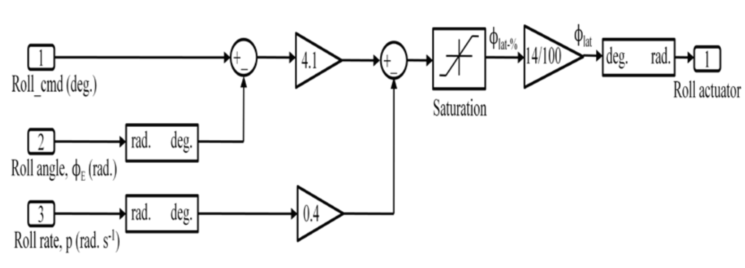

Fig. 9. Roll controller

the inputs to the controller [15–17]. The maximum travel of the roll actuator control rod is 14°. Three nonlinear tracking controllers are designed based on the nonlinear plant model and collective input data are not manipulated by any controller. Proportional integral derivative-based feedback loops for cyclic and rudder commands in percentages are

$$\phi_{lat-\%} = K_1^{lat}(\phi_{cmd} - \phi_E) - K_2^{lat} p \quad (12)$$

$$\theta_{lon-\%} = K_1^{lon}(\theta_{cmd} - \theta_E) - K_2^{lon} q \quad (13)$$

$$\psi_{rud-\%} = K_1^{rud}(\psi_{cmd} - \psi_E) + K_2^{rud}\int(\psi_{cmd} - \psi_E)dt + K_3^{rud} r + K_4^{rud}(d\psi_{cmd}/dt) \quad (14)$$

where ϕ_{cmd}, θ_{cmd}, and ψ_{cmd} are the stick commands, and θ_E, ϕ_E, and ψ_E are the Euler's pitch, roll angle, and yaw angle, respectively. Gain values (K^{lat}, K^{lon}, and K^{rud}) of the proposed controller are estimated in this study. Fig. 10 illustrates the block diagram of the coaxial rotor helicopter in Simulink. For this study, a thrust and torque block set, flapping dynamics block set, force and moment block set, and a 6-degree-of-freedom body dynamics block set are developed to calculate the thrusts and torques produced by the rotors, and the forces acting on the helicopter, and finally, their states [18, 19]. For a fuselage-fixed reference axes system, the Newton–Euler equations of motion are

$$\dot{u} = (X/m) - (wq - vr) - g\sin\theta_E \quad (15)$$

$$\dot{v} = (Y/m) - (ur - wp) + g\cos\theta_E \sin\phi_E \quad (16)$$

$$\dot{w} = (Z/m) - (vp - uq) + g\cos\theta_E \cos\phi_E \quad (17)$$

$$\dot{p} = L/I_{xx} + (I_{yy} - I_{zz})qr/I_{xx} \quad (18)$$

$$\dot{q} = M/I_{yy} + (I_{zz} - I_{xx})rp/I_{yy} \quad (19)$$

$$\dot{r} = N/I_{zz} + (I_{xx} - I_{yy})pq/I_{zz} \quad (20)$$

where $\dot{u}$, $\dot{v}$, $\dot{w}$ are linear accelerations; X, Y, and Z are resultant forces along the body axes; m is the helicopter mass (11.9 kg); $\dot{p}, \dot{q}, \dot{r}$ are angular accelerations; and L, M, and N are the moments of the system. The velocity of the body with respect to the inertial frame is

$$\begin{bmatrix} u^I \\ v^I \\ w^I \end{bmatrix} = R_{rot}(\phi_E, \theta_E, \psi_E)\begin{bmatrix} u \\ v \\ w \end{bmatrix} \quad (21)$$

where $R_{rot}(\phi_E, \theta_E, \psi_E)$ are the rotational matrix and function of the three Euler angles. Eqs. (22)–(24) are the force components along the body axes; Eqs. (25)–(27) are the roll, pitch, and yaw moments about the center of gravity (CG), respectively.

$$X = -T_u\beta_{1c,u} - T_l\beta_{1c,l} + X_f \quad (22)$$

$$Y = T_u\beta_{1s,u} + T_l\beta_{1s,l} - Y_f \quad (23)$$

$$Z = -(T_u + T_l) + Z_f \quad (24)$$

$$L = (K_\beta + T_u h_u)\beta_{1s,u} + (K_\beta + T_l h_l)\beta_{1s,l} \quad (25)$$

$$M = (K_\beta + T_u h_u)\beta_{1c,u} + (K_\beta + T_l h_l)\beta_{1c,l} \quad (26)$$

$$N = Q_l - Q_u \quad (27)$$

Here, X_f, Y_f and Z_f are fuselage drag forces along the x, y, and z axes, respectively; β_{1c}, β_{1s} are longitudinal and lateral flapping angles, respectively; h is rotor height from the CG; and K_β is a rotor hub torsional stiffness factor.

3. System Parameter Identification

System parameter estimation plays an important role because it can significantly affect the controller design of modern complex dynamic systems such as helicopters, airplanes, and space shuttles. The miniature coaxial rotor helicopter used in this study has many physical and aerodynamic parameters. Several of the parameters were measured directly and some were estimated using the flight test data. Measured and estimated parameters for the coaxial

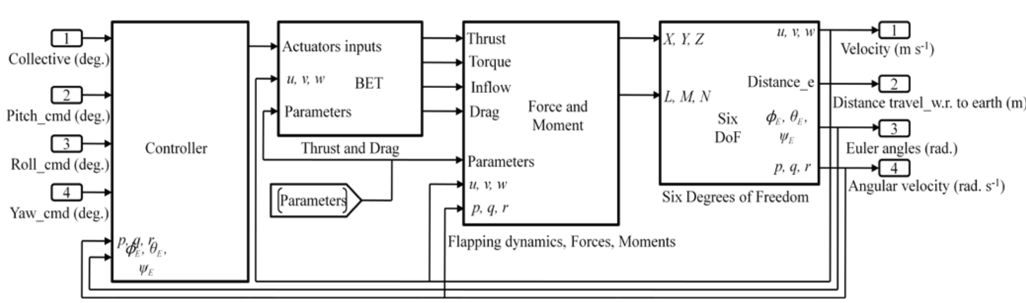

Fig. 10. Developed coaxial rotor model in Matlab-Simulink

DOI: http://dx.doi.org/10.5139/IJASS.2015.16.4.614

rotor model are presented in Tables 1 and 2, respectively. The blades were neither twisted nor tapered. The blade radius, lift curve slope, and chord for the lower rotor were the same as for the upper rotor. Experiments were conducted and flight data were collected for parameter estimation. Collective, longitudinal and lateral cyclic, and rudder were the inputs to the actuators. A flight control computer (FCC) was integrated in the system for manipulating inputs of the controller and for data storage. During forward flight tests, a GPS-INS sensor was used to acquire attitude, velocity, and position data of the helicopter. Fig. 11(a) shows the schematic of the flight system; Fig. 11(b) shows the FCC of the coaxial rotor helicopter. Fig. 12 illustrates a state of the helicopter during the flight test.

Table 1. Measured parameters

Parameter (unit)	Value
Rolling moment of inertia, I_{xx} (kg m^2)	0.14
Pitching moment of inertia, I_{yy} (kg	0.162
Yawing moment of inertia, I_{zz} (kg m^2)	0.133
Flapping moment of inertia (kg m^2)	0.059
Rotor blade radius, R (m)	0.76
Rotor blade chord (m)	0.059
Upper rotor height above CG (m)	0.32
Lower rotor height above CG (m)	0.17
Projected area along x axis (m^2)	0.042
Projected area along y axis (m^2)	0.092
Projected area along z axis (m^2)	0.124
Rotor speed, Ω (rad.s^{-1})	136.1
Motor power (hp)	3.0

Table 2. Identified parameters

Parameter (unit)	Value
Rotor hub torsional stiffness (N m rad.$^{-1}$)	41.3
Lower rotor lon. cyclic to flap gain	0.557
Upper rotor lon. cyclic to flap gain	1.711
Lower rotor lat. cyclic to flap gain	1.376
Upper rotor lat. cyclic to flap gain	0.646
Lat. cyclic proportional gains: K_1^{lat}, K_2^{lat}	4.1, 0.4
Lon. cyclic proportional gains: K_1^{lon}, K_2^{lon}	4.6, 0.4
Rudder PID gains: K_1^{rud}, K_2^{rud}, K_3^{rud}, K_4^{rud}	1.3, 0.13 0.95, 0.2

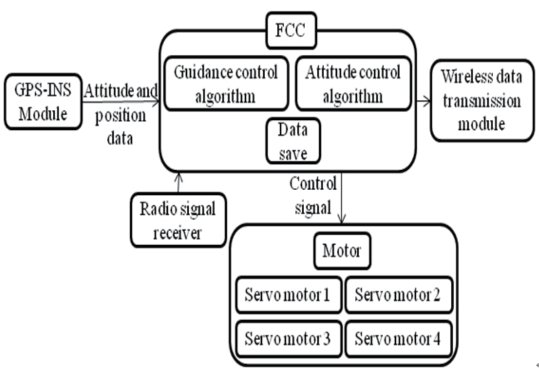

(a)

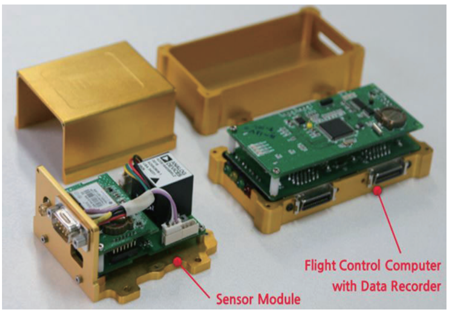

(b)

Fig.11. (a) Schematic of flight system, (b) Flight Control Computer and sensor module

The parameter estimation, optimization, and validation for the coaxial rotor helicopter were performed by using the Matlab Simulink parameter estimation toolbox along with the developed plant model. Collected data of inputs to the actuators as well as flight conditions were considered during simulation. However, external disturbances such as air turbulence were neglected. For computational optimization, several methods are widely used such as gradient descent, nonlinear least squares, and pattern search [20]. Selecting the appropriate method for a specific problem is very important. Since helicopter dynamics are completely nonlinear, the nonlinear least squares method is suitable for this purpose. However, it was found in this study that simulation results often fell into local minima. In contrast, the derivative-free pattern search method gives the global minimum results. The pattern search technique follows exploratory and pattern move steps. Updated base points of the pattern are calculated with Eq. (28):

$$x^{(n+2)} = x^{(n+1)} + \delta[x^{(n+1)} - x^{n}] \quad (28)$$

where x^n (n = 1, 2,...) is the initial point and δ is the step size. Among the derivative-based, derivative-free, and metaheuristic algorithms, the algorithm chosen for an optimization task depends on the type of problem, the proper and efficient performance of the algorithm, and the desired quality of the solution. Although the trust-region reflective algorithm, which estimates the objective function on the

Fig. 12. Coaxial rotor helicopter in flying mode

basis of a truncated Taylor expansion, is a powerful algorithm, it cannot solve underdetermined systems of the nonlinear least squares method. Furthermore, the trust-region reflective algorithm gives local solutions; it was therefore not used. Conversely, the genetic algorithm gives global minima, supports linear, nonlinear, and bound constraints, and uses multiple agents for search. This algorithm follows different steps, such as crossover and mutation, to select the best-fit solution. Hence, during parameter estimation, the pattern search method and genetic algorithm were chosen.

4. Results and Discussion

Figure 13 shows the longitudinal cyclic input, Euler angle, body rate response, and forward velocity determined

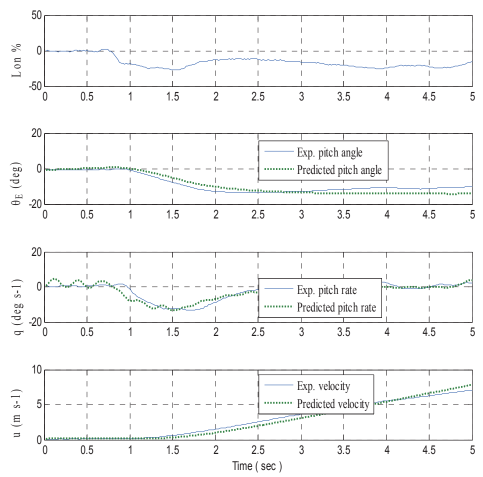

Fig. 13. Comparison of the predicted and experimental data responses during forward flight

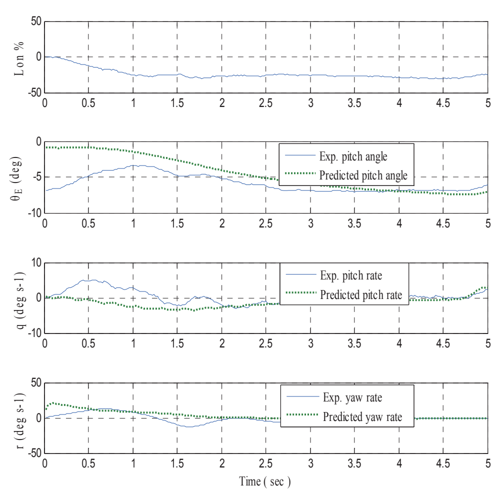

Fig. 14. Validation of the predicted values of different unknown parameters

from flight data, along with simulated results from the parameter estimation. The estimated responses show some discrepancies from actual measurements because of nonlinearity caused by the feedback controller and limitations of the developed numerical plant model. Although the pitch rate from the experimental data and simulation data show some instability of the system, the velocity is well predicted.

A validation task was also performed to verify the predicted values of the unknown parameters. A different data set was used for validation. Fig. 14 shows the validation results, where the first row shows the input to the plant, and the other rows show the predicted responses and experimental data. According to Fig. 14, if the longitudinal input is within 0 to –30.6%, then the pitch attitude shows little discrepancy. In this case, the system velocity reaches 5.52 m.s^{-1}. The estimation as well as validation results show small inconsistencies with the experimental data because of the system's vibration and external disturbances such as wind.

Figures 13 and 14 show that there are uneven fluctuations in the experimental data and slight discrepancies between experimental and simulation data, which result from sensor data-acquisition error and wind gust [21]. The developed numerical plant model does not consider wind gust or load disturbances [16] and the controller has limitations. For the heading, sensor error is 1–2°. Oscillation errors of the experimental data and predicted errors from the plant model can be reduced by using a high-accuracy GPS-INS sensor, and by modifying the developed plant by, for example, including load disturbances.

5. Conclusion

This paper describes the implementation of BET code, investigates and proposes a nonuniform inflow model for the lower rotor of a coaxial rotor helicopter, and validates the model against experimental data. A plant model of the coaxial rotor helicopter was also developed in Matlab Simulink for the analysis of the system attitude, parameter estimation, and controller design in forward flight. A GPS-INS sensor module was incorporated in the helicopter to collect the helicopter state data in real time. An attitude controller was included in the flight control system to tackle the large deviation of attitude response. System parameters were estimated and validated by using different flight data sets. Both sets of results show good agreement with the experimental data. Therefore, the research technique applied in this study can be used for further study of nonuniform inflow models and

DOI: http://dx.doi.org/10.5139/IJASS.2015.16.4.614

system performance. The parameter estimation technique can be useful for estimating unknown parameters during controller design for unmanned aerial vehicles.

Acknowledgments

This work was supported by a National Research Foundation of Korea (NRF) grant funded by the Korean government (MSIP) (No. NRF-2015R1A2A2A01005494), and also by the Human Resource Training Program for Regional Innovation and Creativity through the Ministry of Education and NRF (NRF-2015H1C1A1035499).

References

[1] Leishman, J.G., *Principles of Helicopter Aerodynamics*, Cambridge University press, New York, 2006.

[2] Chen, R.T.N., "A Survey of Nonuniform Inflow Models for Rotorcraft Flight Dynamics and Control Applications," *NASA Technical Memorandum* 102219, 1989.

[3] Mettler, B., Tischler, M.B. and Kanade, T., System identification of small-size unmanned helicopter dynamics, *Journal of the American Helicopter Society*, Vol. 47, No. 1, 2002, pp. 50-63.

[4] Raptis, A. and Valavanis, P., *Linear and nonlinear control of small-scale unmanned helicopters*, Springer, New York, 2011.

[5] Kenneth, W.L., "Aircraft Parameter Estimation," *NASA Technical Memorandum* 88281, 1987.

[6] Abas, N., Legowo, A. and Akmeliawati, R., "Parameter Identification of an Autonomous Quad rotor," *4th International Conference on Mechatronics, Kuala Lumpur*, 2011.

[7] Schafroth, D., Bermes, C., Bouaddallah, S. and Siegwart, R., "Modeling, system identification and robust control of a coaxial micro helicopter," *Control Engineering Practice*, Vol. 18, 2010, pp. 700-711.

[8] Ho-Chan Kim et al., "Parameter Identification and Design of a Robust Attitude Controller Using H Methodology for the Raptor E620 Small-Scale Helicopter," *International Journal of Control, Automation, and Systems*, Vol. 10, No. 1, 2012, pp. 88-101.

[9] Baoquan Song et al., "Dynamic Modeling and Control of a Small-Scale Helicopter," *International Journal of Control, Automation, and Systems*, Vol. 8, No. 3, 2010, pp. 534-543.

[10] Leishman, J.G. and Ananthan, S., "Aerodynamics optimization of a coaxial prop rotor," *Proceedings of 62nd Annual National Forum of the American Helicopter Society*, Phoenix, AZ, 2006.

[11] Prouty, R. W., *Helicopter Performance, Stability*, and Control, Robert E. Krieger Publishing Company, Florida, 1990.

[12] Elliott, J. W., Althoff, S. L. and Sailey, R. H., 1988, Inflow Measurements Made with a Laser Velocimeter on a Helicopter Model in Forward Flight," In three Volumes: volume I: Rectangular plan form at an Advance Ratio of 0.15, *NASA TM 100541*. Volume II: Rectangular plan form at an Advance Ratio of 0.23, NASA TM 100542. Volume III: Rectangular plan form at an Advance Ratio of 0.23, *NASA TM 100543*.

[13] Harrington, R.D., "Full-scale tunnel investigation of the static thrust performance of a coaxial helicopter rotor," *NACA Technical Note 2318*, 1951.

[14] Dingeldein, R.C., "Wind tunnel studies of the performance of a multi rotor configurations," *NACA Technical Note 3236*, 1954.

[15] Ledin, J., *Embedded Control Systems in C/C++*, CMP Books; New York, 2004.

[16] Astrom, K.J. and Hagglund, T., *PID Controllers: Theory, Design, and Tuning*, Instrument Society of America, North Carolina, 1995.

[17] Prasenjit, M. and Steven, L. W., "Modeling and Multivariable Control Technique for Small Coaxial Helicopters," *AIAA Guidance Navigation, and Control Conference*, Portland, August 2011.

[18] J Alejandro, M. T., "Dynamic model for a Coaxial-UAV," *AIAA Modeling and Simulation Technologies (MST) Conference*, Boston, August 2013.

[19] Mettler, B., *Identification modelling and characteristics of miniature rotorcraft*, Kluwer Academic Publishers, Boston, 2003.

[20] Xin-She, Y. and Kozielm, S., Computational optimization, methods and algorithms, Springer, Verlag, 2011.

[21] Harun-Or-Rashid, M., et al., "Unmanned coaxial rotor helicopter dynamics and system parameter estimation", *Journal of Mechanical Science and Technology*, Vol. 28, No. 9, 2014, pp. 3797-3805.

[22] Bramwell, A.R.S., Done, G. and Balmford, D., Bramwell's Helicopter Dynamics, 2nd ed., Butterworth-Heinemann, Oxford, 2001.